A new epidemiological model for the transmission dynamics of Tuberculosis incorporating vaccination and impact of environmental intervention

B.C. Agbata[*], M.O. Fokuo[†], P.A.A. Mensah[†], C.L. Ejikeme[‡], M.B. Okofu[‡], D.C. Ugo[§], W. Obeng-Denteh[¶], D.F. Agbebaku[‡‖], and G.C.E. Mbah[‡]

Abstract

Tuberculosis (TB) remains one of the most lethal infectious diseases globally, with a disproportionate impact on low- and middle-income countries. Its continued transmission is fueled by airborne spread, delayed diagnosis, and inadequate access to treatment. In response, this study develops a comprehensive mathematical model to assess the combined effects of vaccination and environmental interventions on TB transmission dynamics. The model incorporates key control strategies including vaccination, treatment, isolation, improved ventilation, environmental disinfection, and public awareness campaigns. Using the next-generation operator method, the basic reproduction number (R_0) is derived to determine the threshold conditions for disease eradication or persistence. A thorough analytical investigation is carried out to examine the stability of both the disease-free and endemic equilibrium. Numerical simulations conducted in MATLAB confirm the theoretical findings, illustrating that TB can be eliminated when $R_0 < 1$, but persists when $R_0 > 1$. Sensitivity analysis identifies the most impactful parameters, showing that early diagnosis, timely treatment, and environmental improvements significantly reduce disease transmission. This study presents a new integrated modeling approach that incorporates both biomedical interventions and environmental control strategies, offering a more holistic a more holistic and realistic framework for TB control. The proposed model incorporates several critical features including vaccination, treatment, environmental interventions, and re-infection dynamics that are often absent or underrepresented in many existing models. By capturing the complex interactions between these factors, the model provides deeper insights into the mechanisms driving TB transmission and control. Furthermore, the study emphasizes the importance of incorporating localized epidemiological data and realtime surveillance systems to enhance model accuracy and relevance through data fitting. It is recommended that future research should focus on using region-specific parameters and realtime monitoring to guide the development of targeted, evidence-based public health policies aimed at reducing TB burden more effectively.

Keywords and phrases:Mathematical modelling; Sensitivity analysis; Basic reproduction number; Endemic equilibrium; Environmental interventions.

1 Introduction

Tuberculosis (TB) remains one of the most persistent and deadly infectious diseases worldwide, ranking among the top 10 causes of death globally. Caused by the bacterium Mycobacterium tuberculosis, TB

[*]Department of Mathematics and Statistics, Confluence University of Science and Technology, Osara, Nigeria
[†]Mathematics Unit, Department of Mathematics & Information and Communication Technology, St. Ambrose College of Education, Dormaa-Akwamu, Bono Region, Ghana
[‡]Department of Mathematics, University of Nigeria, Nsukka, Nigeria
[§]Department of Mathematical and Statistics Enugu State University of Science and Technology Enugu, Nigeria
[¶]Department of Mathematics, Kwame Nkrumah University of Science and Technology, Kumasi Ghana
[‖]Corresponding Author; E-mail: dennis.agbebaku@unn.edu.ng

primarily affects the lungs but can disseminate to other parts of the body, leading to severe complications if left untreated [1]. According to the World Health Organization (WHO), an estimated 10.6 million people fell ill with TB in 2022, and 1.3 million deaths were reported among HIV-negative individuals, with an additional 167,000 deaths among people living with HIV [2]. These figures underscore the ongoing global health burden posed by TB, particularly in low- and middle-income countries where access to diagnostic and treatment services remains limited. Despite decades of control efforts, TB continues to thrive in regions with poor healthcare infrastructure, high rates of HIV co-infection, and socio-economic instability [3]. One of the major challenges in combating TB is its airborne mode of transmission, which allows the pathogen to spread easily in crowded or poorly ventilated environments [4]. Additionally, the rise of multidrug-resistant TB (MDR-TB) and extensively drug-resistant TB (XDR-TB) has made treatment more complex and less effective [5]. Studies indicate that MDR-TB accounted for nearly half a million new cases in 2022 alone, with treatment success rates hovering around 60% globally [2]. Delayed diagnosis and inconsistent treatment adherence remain critical hurdles in TB control. Many individuals with latent TB infection (LTBI) do not exhibit symptoms and thus go undiagnosed, while others discontinue treatment prematurely due to drug side effects or economic constraints [6]. According to recent modeling studies, delayed treatment initiation can significantly contribute to ongoing community transmission and increased mortality [7]. Public health systems often struggle to maintain efficient TB surveillance, especially in areas affected by political conflict or humanitarian crises, further exacerbating disease spread [8].

Vaccination remains a vital tool in the global fight against TB. The Bacillus Calmette-Guérin (BCG) vaccine, though widely used, offers limited protection, especially against pulmonary TB in adults [9]. Current research is focused on developing more effective TB vaccines, such as the M72/AS01E candidate, which has shown promise in recent phase IIb trials [10]. Meanwhile, non-pharmaceutical interventions, including public awareness, environmental controls, and infection prevention measures, are increasingly being emphasized as complementary strategies to reduce TB transmission in high-burden settings [11]. Mathematical modeling has emerged as an essential tool in understanding TB dynamics and guiding policy decisions. Models help simulate the impact of various interventions, identify critical thresholds for disease elimination, and assess resource allocation strategies [12]. Recent studies have integrated both biomedical and environmental control measures into TB transmission models, highlighting the importance of a multidisciplinary approach to TB control [13]. This study builds upon that foundation by developing a robust mathematical model that incorporates vaccination and environmental interventions to explore their combined effects on TB transmission within a human population. Barman et al. [14] developed a hybrid modeling framework known as Epidemic-Guided Deep Learning (EGDL) to forecast the spatiotemporal spread of tuberculosis across Japan. The model integrated a mechanistic SIR-type compartmental structure with deep neural networks, incorporating factors such as saturated incidence, demographic heterogeneity, and mobility through graph diffusion. Using TB case data from 47 Japanese prefectures, the authors validated their approach and demonstrated that EGDL outperformed traditional statistical models in terms of accuracy and robustness. The model also included a Bayesian uncertainty quantification feature, enabling predictions with confidence intervals. Their results showed that the EGDL model successfully captured TB dynamics and could adapt to changes in regional transmission patterns. The study concluded that combining mechanistic models with deep learning provides a powerful tool for forecasting and guiding public health interventions against TB. Barman et al. introduced an innovative Epidemic-Guided Deep Learning (EGDL) framework that combined a mechanistic SIR model with neural networks to forecast the spatial spread of tuberculosis across Japan. While their model was highly accurate and included advanced features like Bayesian uncertainty quantification, it primarily emphasized data-driven forecasting and did not deeply incorporate the real-world public health interventions necessary for TB control. The new study improves upon this by offering a deterministic, mechanistically interpretable model that integrates critical biomedical and environmental interventions-including vaccination, treatment, reinfection, and sanitation. By focusing not only on prediction but also on control strategy evaluation, the new model provides deeper insights into how various interventions reduce TB transmission, some-

thing the EGDL framework did not explicitly address. Kasereka [15] developed a multi-level hybrid model that coupled an 8-compartment equationbased model (EBM) with an agent-based model (ABM) to simulate TB spread in urban populations with inter-city mobility. The model incorporated key epidemiological states, including latent infection and chronic TB, and allowed for individual agents to travel between cities. Simulations revealed that inter-city movement substantially influenced TB transmission dynamics, even when local transmission rates were low. The study highlighted how mobility could undermine local control efforts if not addressed at a systemic level. Kasereka concluded that TB control strategies should not be implemented in isolation but should rather consider human mobility patterns and coordination between regions. Kasereka's multi-level hybrid model effectively captured TB dynamics influenced by inter-city mobility using an agent-based and equation-based approach. However, the model primarily focused on movement-driven spread and lacked a comprehensive integration of public health interventions such as treatment coverage, vaccination efforts, or environmental sanitation. In contrast, the new study presents a more intervention-focused model that incorporates these critical factors, alongside reinfection dynamics, which better reflects the reality of TB control in high-burden settings. Additionally, the use of data fitting and parameter sensitivity analysis in the new model offers a stronger foundation for targeted policy development and health resource allocation than the mobilityfocused approach alone. Xu et al. [16] formulated a compartmental TB transmission model tailored to the Chinese population, incorporating latent infection and BCG vaccination. The model was calibrated using real incidence data, and a vaccination-adjusted reproduction number (Rv/mathcal $\{R\}$_v) was derived to assess disease persistence. Sensitivity analysis revealed that vaccination rate and vaccine effectiveness were the most influential parameters in reducing transmission, with correlation coefficients of -0.81 and -0.825 respectively. Their model estimated $R_V = 0.4442$, suggesting that under current vaccination coverage and treatment levels, TB could be significantly suppressed in China. The authors concluded that enhancing vaccine delivery and public health awareness would be crucial for meeting WHO TB elimination targets. Xu et al. developed a compartmental TB model centered on BCG vaccination and latent infections in China, successfully highlighting the impact of vaccination and vaccine efficacy. While their model was rigorous and well-calibrated using actual incidence data, it was limited in scope as it did not include environmental interventions or reinfection pathways. The new study expands on this by adopting a more comprehensive framework that includes not just vaccination and treatment, but also environmental disinfection and reinfection, thus providing a more realistic and holistic view of TB transmission. Moreover, the new study's emphasis on local data fitting and real-time surveillance enhances its applicability for public health decision-making, beyond what was addressed in Xu et al.'s vaccination-centric model.

Abonyo and Okeyo [17] formulated a SEIRS model incorporating environmental transmission pathways to evaluate TB control strategies. The model included compartments for susceptible, exposed, infectious, and recovered individuals and introduced three time-dependent control functions: vaccination, treatment, and isolation. The authors applied optimal control theory and conducted simulations using Kenya's TB incidence data from 2000 to 2022. Their findings demonstrated that optimal implementation of treatment and isolation could reduce TB prevalence significantly while remaining cost-effective. The study emphasized that a combined strategy involving early diagnosis, prompt treatment, and improved environmental sanitation was critical for controlling TB spread. They concluded that in resource-limited settings, mathematical models should guide cost-effective policy development. Abonyo and Okeyo formulated a SEIRS model that incorporated environmental transmission and applied optimal control theory to evaluate TB interventions in Kenya. While their model accounted for environmental effects and included vaccination, treatment, and isolation as time-dependent controls, it did not consider re-infection dynamics or data fitting for real-time policy guidance. The new study improves on this by including a broader range of compartments, integrating reinfection loops, and promoting data-driven decision-making through the fitting of localized incidence data. It also underscores the importance of real-time surveillance and region-specific modeling, making it more adaptable and impactful for resource-constrained settings. Akinyemi et al. [18] developed a compartmental model to analyze TB transmission dynamics in Nigeria, focusing on the impact of vaccination and treat-

ment strategies. The model included key population groups: susceptible, exposed, infectious, chronic, treated, and recovered individuals. Simulations showed that while vaccination gradually reduced the susceptible population, treatment interventions had a more immediate and pronounced effect on reducing the chronic TB burden. Sensitivity analysis confirmed treatment as the most influential factor in the model. The study concluded that for high-burden settings like Nigeria, improving access to treatment and ensuring patient compliance are critical for effective TB control. The authors recommended strengthening diagnostic services, expanding vaccination outreach, and maintaining consistent treatment protocols. Akinyemi et al. developed a model tailored to TB transmission in Nigeria, focusing mainly on the roles of vaccination and treatment. Their study effectively identified treatment as a key driver for reducing TB burden. However, the model lacked environmental components, re-infection mechanisms, and a data-fitting framework that would improve predictive performance. The new study addresses these gaps by incorporating environmental interventions, re-infection pathways, and sensitivity-based policy prioritization. It also recommends the use of real-time, localized data to ensure the model remains applicable across diverse epidemiological landscapes. These additions significantly enhance the model's utility for long-term TB control in high-burden regions like Nigeria.

The primary aim of this study is to develop and analyze a novel epidemiological model that captures the transmission dynamics of tuberculosis (TB) by incorporating the combined effects of vaccination, treatment, re-infection, and environmental interventions. This integrated approach seeks to offer a more holistic and realistic framework for understanding and controlling TB, particularly in settings where both biomedical and environmental factors significantly influence disease spread. To achieve this aim, the study formulates a deterministic compartmental model that subdivides the human population into key classes based on disease status. The model's mathematical validity is established by investigating the existence of an invariant region and the positivity of solutions, ensuring that the model remains biologically meaningful. A critical threshold parameter the basic reproduction number (R_0)-is derived to assess the potential for disease persistence or elimination. Furthermore, both local and global stability analyses are conducted to evaluate the behavior of the disease-free and endemic equilibria under various conditions. Sensitivity analysis is performed to identify the most influential parameters affecting TB transmission and control, thereby aiding in prioritizing intervention efforts. To enhance the practical relevance of the model, it is fitted to real epidemiological data using appropriate estimation techniques. Finally, numerical simulations are carried out to assess the effectiveness of different control strategies, including vaccination coverage, treatment rates, and environmental measures such as improved ventilation or reduced overcrowding. Through these comprehensive analyses, the study aims to support the design of more targeted and effective public health policies for TB control.

Despite significant advancements in tuberculosis (TB) control strategies, the disease remains a persistent global health threat, particularly in low- and middle-income countries. Numerous mathematical models have been developed to understand the transmission dynamics of TB, yet many of these models primarily focus on biomedical interventions such as treatment and vaccination, often neglecting the broader environmental and structural factors that influence disease spread. Moreover, the re-infection of treated individuals and the influence of environmental interventions such as ventilation improvement, overcrowding reduction, and sanitation are frequently underrepresented or omitted altogether in conventional models. Another critical gap in the existing literature is the limited integration of real-time epidemiological data and region-specific parameters, which are essential for generating accurate and context-sensitive predictions. Without these features, the effectiveness of many TB models is constrained, especially in their ability to inform localized public health policies.

This study is motivated by the need for a more comprehensive and realistic approach to TB modeling one that captures the multifactorial nature of transmission and control. By incorporating key elements such as vaccination, treatment, re-infection, and environmental interventions into a deterministic compartmental model, this research aims to fill the gaps left by previous models. Additionally, the model emphasizes the role of data fitting and localized surveillance, reinforcing the importance of tailoring intervention strategies to specific epidemiological contexts. The ultimate goal is to support the development of evidence-based, regionally adaptive policies that can more effectively reduce the burden

of TB.

2 Analysis of Tuberculosis Vaccination model

2.1 Model Formulation

A deterministic compartmental model on the transmission dynamics of Tuberculosis is proposed. We sub-divided the total human population $N_H(t)$, into six (6) distinct classes of susceptible humans S_H, exposed humans to TB only E_T acutely infected humans with TB only A_T, chronically infected humans with TB only C_T, Treated humans due to TB only T_T, and Recovered humans R from this disease. The recruitment rate of humans into the susceptible population is at the rate of Λ_H so that β_T is the effective contact rate with the probability of infection per contact with infected human with TB.,. The rate at which individuals exposed to TB is given as $\theta_T \cdot \tau$ is the rate at which an acutely infected human with TB progresses to been chronically infected with TB. Also, the treatment rate of humans infected with acute TB, chronic TB is given as γ_T, γ_C respectively. The rate of recovery of humans from TB is given at the rate of α_T. The natural death rate of humans is given as μ_H. The disease induced death rate of humans due to TB infection is given as δ_T and σ_T is the vaccination rate whereas ψ_T is the progress rate from vaccinated class to exposed class. The impact of environmental intervention is ω and ξ_T is the immunity waning rate of partially immune humans.

The model equations

$$\frac{dS_H}{dt} = \Lambda_H + \varsigma_T R - ((1-\omega)\lambda_T + \sigma_T + \mu_H)\, S_H \tag{1}$$

$$\frac{dV_H}{dt} = \sigma_T S_H - (\psi_T + \mu_H)\, V_H \tag{2}$$

$$\frac{dE_T}{dt} = (1-\omega)\lambda_T S_H + \psi_T V_H - (\theta_T + \mu_H)\, E_T \tag{3}$$

$$\frac{dA_T}{dt} = \theta_T E_T - (\tau + \gamma_T + \delta_T + \mu_H)\, A_T \tag{4}$$

$$\frac{dC_T}{dt} = \tau A_T - (\gamma_c + \delta_T + \mu_H)\, C_T \tag{5}$$

$$\frac{dT_T}{dt} = \gamma_T A_T + \gamma_C C_T - (\alpha_T + \delta_T + \mu_H)\, T_T \tag{6}$$

$$\frac{dR}{dt} = \alpha_T T_T - (\varsigma_T + \mu_H)\, R \tag{7}$$

The force of infection for the Tuberculosis model is given as: $\lambda_T = \frac{\beta_T(\eta_1 A_T + \eta_2 C_T + \eta_3 T_T)}{N_H}$

Model flow diagram is shown in Figure 1.

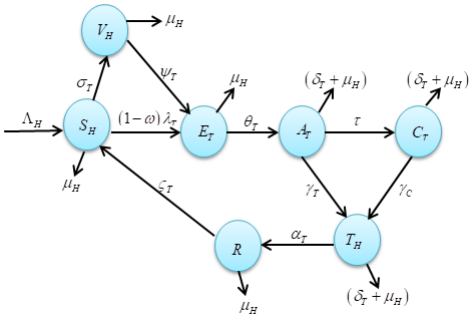

Figure 1: Schematic diagram for the TB-Only Model

Table 1 and Table 2 gives a summary of the description of the variables and parameter used in the model.

Table 1: Description of variables used the model

Variables	Description
Susceptible humans	S_H
Vaccinated humans	V_H
Exposed Humans to TB	E_T
Acutely infected humans with TB	A_T
Chronically infected humans with TB .	C_T
Treated Humans to TB	T_T
Recovered Humans	R

Table 2: Description of parameters used the model

Parameters	Description
Λ_H	Recruitment rate of humans
σ_T	Vaccination rate
ω	Environmental interventions
ζ_T	Immunity waning rate of partially immune humans
θ_T	Progression rate of exposed TB to acutely infected TB class
β_T	Contact rate
ψ_T	Progression rate from vaccinated to exposed class
η_1, η_2, η_3	Modification parameters
μ_H	Natural death rate of humans
γ_T	Treatment rate of infected humans with TB
τ	Progression rate from acute TB to chronic TB class
δ_T	Disease induced death rate of infected acute TB, chronic TB
α_T	Recovery rate of infected individuals.

3 Invariant Region of the Tuberculosis Model

The solutions of the proposed tuberculosis model are said to be epidemiologically feasible for all $t > 0$ if they remain non-negative and bounded in a biologically meaningful region D. We define this region as:

$$D = (S_H, V_H, E_T, A_T, C_T, T_T, R) \in R_+^7 : N_H \leq \frac{\Lambda_H}{\mu_H} \tag{8}$$

3.0.1 Proof of invariant region

Let the total human population at time t be:

$$N_H(t) = S_H(t) + V_H(t) + E_T(t) + A_T(t) + C_T(t) + T_T(t) + R(t)$$

Summing the right-hand sides of all the differential equations governing the compartments, we get

$$\frac{dN_H}{dt} = \frac{dS_H}{dt} + \frac{dV_H}{dt} + \frac{dE_T}{dt} + \frac{dA_T}{dt} + \frac{dC_T}{dt} + \frac{dT_T}{dt} + \frac{dR}{dt} \tag{9}$$

This simplifies to:

$$\frac{dN_H}{dt} = \Lambda_H - \mu_H N_H - \delta_T \left(A_T + C_T + T_T\right).$$

Since

$$\delta_T \left(A_T + C_T + T_T\right) \geq 0,$$

it follows that

$$\frac{dN_H}{dt} \leq \Lambda_H - \mu_H N_H.$$

We now solve this differential inequality using the integrating factor method. Consider the equation

$$\frac{dN_H}{dt} + \mu_H N_H \leq \Lambda_H.$$

Multiplying both sides by the integrating factor $e^{\mu_H t}$, we obtain:

$$\frac{d}{dt}\left(N_H e^{\mu_H t}\right) \leq \Lambda_H e^{\mu_H t}.$$

Integrating both sides from 0 to t we have

$$N_H(t)e^{\mu_H t} - N_H(0) \leq \frac{\Lambda_H}{\mu_H}\left(e^{\mu_H t} - 1\right).$$

Thus

$$N_H(t) \leq \frac{\Lambda_H}{\mu_H} + \left(N_H(0) - \frac{\Lambda_H}{\mu_H}\right) e^{-\mu_H t}.$$

Taking the limit as $t \to \infty$, we get

$$\limsup_{t\to\infty} N_H(t) \leq \frac{\Lambda_H}{\mu_H}.$$

Therefore, the total population remains bounded above by Λ_H/μ_H, which implies that all compartment values remain non-negative and the solution trajectories enter and stay in the region D.

By applying Birkhoff and Rota's theorem, it follows that the region:

$$D = \left\{(S_H, V_H, E_T, A_T, C_T, T_T, R) \in R_+^7; N_H(t) \leq \frac{\Lambda_H}{\mu_H}\right\}$$

is positively invariant under the flow generated by the tuberculosis model. Hence, any solution starting in D remains in D for all $t > 0$ [31]. This confirms that the tuberculosis model is epidemiologically and mathematically well-posed.

4 Positivity of Solutions of the Tuberculosis Model

To ensure that the tuberculosis model is epidemiologically and mathematically well-posed, it is necessary to prove that all state variables of the model are nonnegative for all $t > 0$ in a feasible region D, defined as

$$D = \left\{(S_H, V_H, E_T, A_T, C_T, T_T, R) : S_H > 0, V_H > 0, E_T > 0, A_T > 0, C_T > 0, T_T > 0, R > 0, \frac{\Lambda_H}{\mu_H} \geq N_H\right\}.$$

Lemma 4.1. *Let the initial data for the tuberculosis model be*

$$(S_H(0), V_H(0), E_T(0), A_T(0), C_T(0), T_T(0), R(0)) > 0.$$

Then, the solutions $(S_H, V_H, E_T, A_T, C_T, T_T, R)$ *of the model remain positive for all* $t > 0$.

Proof. Let
$t = \sup t > 0 : S_H > 0, V_H > 0, E_T > 0, A_T > 0, C_T > 0, T_T > 0, R > 0$ for $t \in [0, t]$.
Thus, $t > 0$. From the first equation of the model:
$\frac{dS_H}{dt} = \Lambda_H + \varsigma_T R - ((1-\omega)\lambda_T + \sigma_T + \mu_H)\, S_H$,
we can observe that:
$\frac{dS_H}{dt} \geq -((1-\omega)\lambda_T + \sigma_T + \mu_H)\, S_H$.
Since all terms in the parentheses are nonnegative, denote
$c = (1-\omega)\lambda_T + \sigma_T + \mu_H > 0$.

Then:
$\frac{dS_H}{dt} \geq -cS_H$.
Rewriting this inequality:
$\frac{1}{S_H}\frac{dS_H}{dt} \geq -c$.
Integrating both sides:
$\int \frac{1}{S_H}, dS_H \geq -\int c, dt$,
which yields:
$\ln S_H \geq -ct + C_1$,
where C_1 is the integration constant. Exponentiating both sides:
$S_H(t) \geq C_1 e^{-ct}$.

Applying the initial condition $S_H(0) = C_1$:
$S_H(t) \geq S_H(0)e^{-ct} \geq 0$.

Since $c > 0$, we conclude $S_H(t) > 0$ for all $t > 0$.

Similarly, it can be shown that all other compartments ($V_H, E_T, A_T, C_T, T_T, R$) remain positive by following the same approach [29, 30]. Thus, all state variables of the tuberculosis model are nonnegative for all $t > 0$, proving that the model is well-posed within the feasible region D.

5 Asymptotic Stability of the Disease-Free Equilibrium of the Tuberculosis Model

The disease-free equilibrium (DFE) represents the steady state where there is no infection, i.e., $E_T = A_T = C_T = T_T = R = 0$. This point reflects the complete absence of the disease within the population. For the tuberculosis model, the DFE is given as:

$$E_0 = \left(S_H^0, V_H^0, E_T^0, A_T^0, C_T^0, T_T^0, R_T^0\right) = \left(\frac{\Lambda_H}{Q_1}, \frac{\sigma_T \Lambda_H}{\mu_H Q_1}, 0, 0, 0, 0, 0\right) \text{ Where } Q_1 = \sigma_T + \mu_H \quad (6)$$

6 Basic Reproduction Number of the tuberculosis Model

The basic reproduction number R_0 is defined as the expected number of secondary infections produced by a single infected individual in a completely susceptible population [27, 28]. It is a threshold quantity that determines whether the infection can invade and persist in the population. If $\mathrm{R}_0 < 1$, the infection dies out; if $\mathrm{R}_0 > 1$, the infection can spread.

Let the matrices F and V be:

$$F = \begin{bmatrix} 0 & \frac{(1-\omega)\eta_1\mu_H}{Q_1} & \frac{(1-\omega)\eta_2\mu_H}{Q_1} & \frac{(1-\omega)\eta_3\mu_H}{Q_1} \\ 0 & 0 & 0 & 0 \\ 0 & 0 & 0 & 0 \\ 0 & 0 & 0 & 0 \end{bmatrix}, V = \begin{bmatrix} P_2 & 0 & 0 & 0 \\ -\theta_T & P_3 & 0 & 0 \\ 0 & -\tau & P_4 & 0 \\ 0 & -\gamma_T & -\gamma_C & P_5 \end{bmatrix}.$$

$$FV^{-1} = \begin{bmatrix} \frac{\theta_T(F_1P_4P_5+F_2\tau P_5+F_3P_4\gamma_T+F_3\tau\gamma_C)}{P_2P_3P_4P_5} & \frac{F_1P_4P_5+F_2\tau P_5+F_3P_4\gamma_T+F_3\tau\gamma_C}{P_4P_3P_5} & \frac{F_2}{P_4}+\frac{F_3\gamma_C}{P_4P_5} & \frac{F_3}{P_5} \\ 0 & 0 & 0 & 0 \\ 0 & 0 & 0 & 0 \\ 0 & 0 & 0 & 0 \end{bmatrix}$$

The inverse of V, denoted V^{-1}, is computed analytically or numerically. The nextgeneration matrix is then obtained as $K = FV^{-1}$, and the basic reproduction number R_0 is the spectral radius (dominant eigenvalue) of K : $\mathrm{R}_0 = \rho\left(FV^{-1}\right)$.

$$\frac{\theta_T\left(F_1P_4P_5 + F_2\tau P_5 + F_3P_4\gamma_T + F_3\tau\gamma_C\right)}{P_2P_3P_4P_5} \quad (7)$$

Where, $F_1 = \frac{(1-\omega)\eta_1\mu_H}{Q_1}, F_2 = \frac{(1-\omega)\eta_2\mu_H}{Q_1}, F_3 = \frac{(1-\omega)\eta_3\mu_H}{Q_1}$,

$$P_1 = (\psi_1 + \mu_H), P_2 = (\theta_T + \mu_H), P_3 = (\tau + \gamma_T + \delta_T + \mu_H)$$
$$P_4 = (\gamma_C + \delta_T + \mu_H), P_5 = (\alpha_T + \delta_T + \mu_H), P_6 = (\varsigma_T + \mu_H)$$

7 Global Asymptotic Stability of the Disease Free Equilibrium Point of the Tuberculosis Model

To investigate the global stability of the disease free equilibrium, we use the technique implemented by Castillo-Chavez and Song, To do this, we write the equation in the uninfected class as $\frac{dX}{dt} = F(X, Z)$

And we re-write the equation in the infected class as $\frac{dZ}{dt} = G(X, Z)$

Where $X = (S_H, V_H, R) \in R^3_+$ denotes the uninfected population and $Z = (E_T, A_T, C_T, T_T) \in R^4_+$ denotes the infected population [25, 26].

$\eta_0 = (X^*, 0)$ represents the disease free equilibrium point of the system, and it is globally asymptotically stable if it satisfies the following conditions:

$$H_1 : \frac{dX}{dt} = F(X^*, 0), X^* \text{ is globally asymptotically stable}$$
$$H_2 : \frac{dZ}{dt} = D_Z G(X^*, 0) Z - \hat{G}(X, Z)$$

$\hat{G}(X, Z) \geq 0$ for all $(X, Z) \in D$ and where $D_Z G(X'0)$ is an M-matrix (i.e., the diagonal elements are non-negative) and it is also the Jacobian of $G(X, Z)$ evaluated at ($X'0$).

If the system satisfies the above condition, then the theorem below holds [24].

Theorem 7.1. *The equilibrium point $\eta_0 = (X^*, 0)$ is globally asymptotically stable if $R_0 \leq 1$.*

Proof. Let's define: $F(X, Z) = \begin{bmatrix} \Lambda_H + \varsigma_T R - ((1-\omega)\lambda_T + \sigma_T + \mu_H) S_H \\ \sigma_T S_H - (\psi_T + \mu_H) V_H \\ \alpha_T T_T - (\varsigma_T + \mu_H) R \end{bmatrix}$

$$G(X, Z) = \begin{bmatrix} \frac{\beta_T(\eta_1 A_T + \eta_2 C_T + \eta_3 T_T)}{N_H}(1-\omega) S_H + \psi_T V_H - (\theta_T + \mu_H) E_T \\ \theta_T E_T - (\tau + \gamma_T + \delta_T + \mu_H) A_T \\ \tau A_T - (\gamma_C + \delta_T + \mu_H) C_T \gamma \\ T_T^{A_T + \gamma_C C_T - (\alpha_T + \delta_T + \mu_H) T_T} \end{bmatrix}$$

At disease free equilibrium

$$H_1 : \frac{dS_H}{dt} = \Lambda_H + \varsigma_T R - (\sigma_T + \mu_H) S_H \frac{dV_H}{dt} = \sigma_T S_H - (\psi_T + \mu_H) V_H \frac{dR}{dt} = -(\varsigma_T + \mu_H) R$$
$$H_2 : D_Z G(X^*, 0) Z = \begin{bmatrix} \beta_T(1-\omega)(\eta_1 A_T + \eta_2 C_T + \eta_3 T_T) - (\theta_T + \mu_H) E_T \\ \theta_T E_T - (\tau + \gamma_T + \delta_T + \mu_H) A_T \tau A_T - (\gamma_C + \delta_T + \mu_H) C_T \\ \gamma_T A_T + \gamma_C C_T - (\alpha_T + \delta_T + \mu_H) T_T \end{bmatrix}$$

Let's define: $\hat{G}(X, Z) = D_Z G(X^*, 0) Z - G(X, Z)$

$$\hat{G}(X, Z) = \begin{bmatrix} \beta_T(1-\omega)(\eta_1 A_T + \eta_2 C_T + \eta_3 T_T)\left(1 - \frac{S_H}{N_H}\right) \\ 0 \\ 0 \\ 0 \end{bmatrix} \tag{8}$$

Clearly, $1 \geq \frac{S_H}{N_H}$ this implies that $\hat{G}(X, Z) \geq 0$.

Therefore, the disease-free equilibrium of the Tuberculosis model is globally asymptotically stable when $R_0 \leq 1$.

8 Endemic Equilibrium Point of the Tuberculosis Model

The endemic equilibrium point is the steady state where there is persistence or prevalence of disease in the population.

Theorem 8.1. *The endemic equilibrium point of the Tuberculosis model is stable if* $R_0 > 1$ *and unstable if* $R_0 < 1$.

Proof. To obtain the endemic equilibrium, we set the right-hand side of the differential equations to zero and solve for the state variables.

Thus, at the endemic equilibrium point: $\frac{dS_H}{dt} = \frac{dV_H}{dt} = \frac{dE_T}{dt} = \frac{dA_T}{dt} = \frac{dC_T}{dt} = \frac{dT_T}{dt} = \frac{dR}{dt} = 0$.

Let $\eta^* = (S_H^*, V_H^*, E_T^*, A_T^*, C_T^*, T_T^*, R^*)$ be the endemic equilibrium point.

Let's define:

$$W_1 = (\theta_T + \mu_H), W_2 = (\tau + \gamma_T + \delta_T + \mu_H), W_3 = (\gamma_c + \delta_T + \mu_H), W_4 = (\alpha_T + \delta_T + \mu_H)$$
$$W_5 = (\varsigma_T + \mu_H), W_6 = (\psi_T + \mu_H), W_7 = ((1-\omega)\lambda_T + \sigma_T + \mu_H)$$

By making each compartment the subject of the formula when each equation in (1) - (7) is equated to zero, we obtain:

$\Lambda_H + \varsigma_T R^* - ((1-\omega)\lambda_T^* + \sigma_T + \mu_H) S_H^* = 0$

$$\implies S_H^* = \frac{\Lambda_H + \varsigma_T R^*}{(1-\omega)\lambda_T^* + \sigma_T + \mu_H} \tag{10}$$

$\sigma_T S_H^* - (\psi_T + \mu_H) V_H^* = 0$

$$\implies V_H^* = \frac{\sigma_T S_H^*}{W_6} \tag{11}$$

$(1-\omega)\lambda_T^* S_H^* + \psi_T V_H^* - (\theta_T + \mu_H) E_T^* = 0$

$$\implies E_T^* = \frac{(1-\omega)\lambda_T^* S_H^* + \psi_T V_H^*}{W_1} \tag{12}$$

$\theta_T E_T^* - (\tau + \gamma_T + \delta_T + \mu_H) A_T^* = 0$

$$\implies A_T^* = \frac{\theta_T E_T^*}{W_2} \tag{13}$$

$\tau A_T^* - (\gamma_c + \delta_T + \mu_H) C_T^* = 0$

$$\implies C_T^* = \frac{\tau A_T^*}{W_3} \tag{14}$$

$\gamma_T A_T^* + \gamma_C C_T^* - (\alpha_T + \delta_T + \mu_H) T_T^* = 0$

$$\implies T_T^* = \frac{\gamma_T A_T^* + \gamma_C C_T^*}{W_4} \tag{15}$$

$\alpha_T T_T^* - (\varsigma_T + \mu_H) R^* = 0$

$$\implies R^* = \frac{\alpha_T T_T^*}{W_5}. \tag{16}$$

We observe that these equations are expressed in terms of each other.

In (16), R^* is expressed in terms of T_T^*.That is, $R^* = \frac{\alpha_T T_T^*}{W_5}$.

Substituting for R^* in equation (10) we expressed S_H^* in terms T_T^*. That is,

$$S_H^* = \frac{\Lambda_H + \varsigma_T \frac{\alpha_T T_T^*}{W_5}}{(1-\omega)\lambda_T^* + \sigma_T + \mu_H} = \frac{\Lambda_H W_5 + \varsigma_T \alpha_T T_T^*}{W_5\left((1-\omega)\lambda_T^{**} + \sigma_T + \mu_H\right)}$$

In (10), we expressed V_H^* in terms of S_H^* : $V_H^* = \frac{\sigma_T S_H^*}{W_6}$

In (11), we expressed E_T^* in terms of S_H^* and V_H^* : $E_T^* = \frac{(1-\omega)\lambda_T^* S_H^* + \psi_T V_H^{**}}{W_1}$

In (12), we expressed A_T^* in terms of E_T^* : $A_T^* = \frac{\theta_T E_T^*}{W_2}$

In (13), we expressed C_T^* in terms of A_T^* : $C_T^* = \frac{\tau A_T^*}{W_3}$

In (14), we expressed T_T^* in terms of A_T^* and C_T^* : $T_T^* = \frac{\gamma_T A_T^* + \gamma_C C_T^*}{W_4}$

Now, let's substitute also into the force of infection: $\lambda_T^* = \frac{\beta_T\left(\eta_1 A_T^* + \eta_2 C_T^* + \eta_3 T_T^*\right)}{N_H^{**}}$

After further algebraic substitutions and simplifications, we get an expression for λ_T^* of the form:

$$\lambda_T^* = \frac{W_1 W_2 W_3 W_4 W_5 W_6 W_7 \mu_H \left(R_0 - 1\right)}{D}$$

Where,

$$D = \left(W_5 W_3 W_4 \left(\theta_T + W_1\right) + W_1 W_5 W_3 W_4\right)\mu_H + W_5 W_3 \gamma_t \theta_t \left(\mu_h + \alpha_t\right) + W_5 \tau W_2 W_4 \left(\mu_h + \gamma_k\right) \quad (9)$$

Thus, for λ_T^* to be positive at the endemic equilibrium point, we need $R_0 - 1 > 0. \Rightarrow R_0 > 1$ and the endemic equilibrium point is stable.

9 Sensitivity Analysis for the Tuberculosis Model

The sensitivity index of the reproduction number with respect to any parameter p is given by:

$$\begin{aligned}
\mathfrak{J}_p^{R_0} &= \frac{\partial R_0}{\partial p} \times \frac{p}{R_0}, \\
\mathfrak{J}_{\beta_T}^{\mathrm{R}_0} &= 1, \\
\mathfrak{J}_{\theta_T}^{\mathrm{R}_0} &= 1 - \frac{\theta_T}{P_2}, \\
\mathfrak{J}_{\tau}^{\mathrm{R}_0} &= \frac{F_2 P_5 + F_3 \gamma_C}{F_1 P_4 P_5 + F_2 \tau P_5 + F_3 P_4 \gamma_T + F_3 \tau \gamma_C} \cdot \tau, \\
\mathfrak{J}_{\gamma_T}^{\mathrm{R}_0} &= \frac{F_3 P_4}{F_1 P_4 P_5 + F_2 \tau P_5 + F_3 P_4 \gamma_T + F_3 \tau \gamma_C} \cdot \gamma_T - \frac{\gamma_T}{P_3}, \\
\mathfrak{J}_{\alpha_T}^{\mathrm{R}_0} &= -\frac{\alpha_T}{P_5}, \\
\mathfrak{J}_{\omega}^{\mathrm{R}_0} &= -\frac{\omega}{1-\omega}, \\
\mathfrak{J}_{\eta_1}^{\mathrm{R}_0} &= \frac{\eta_1 F_1^{-1} \cdot F_1 P_4 P_5}{\mathrm{N}} = \frac{\eta_1}{F_1} \cdot \frac{F_1 P_4 P_5}{\mathrm{N}} = \frac{\eta_1 P_4 P_5}{\mathrm{N}}, \\
\mathfrak{J}_{\eta_2}^{\mathrm{R}_0} &= \frac{\eta_2 \tau P_5}{\mathrm{N}}, \\
\mathfrak{J}_{\eta_3}^{\mathrm{R}_0} &= \frac{\eta_3 \left(P_4 \gamma_T + \tau \gamma_C\right)}{\mathrm{N}}, \\
\mathfrak{J}_{\sigma_T}^{\mathrm{R}_0} &= -\frac{\sigma_T}{Q_1} \\
\mathfrak{J}_{\gamma_C}^{\mathrm{R}_0} &= \frac{F_3 \tau}{\mathrm{N}} \cdot \gamma_C - \frac{\gamma_C}{P_4}, \\
\mathfrak{J}_{\psi_T}^{\mathrm{R}_0} &= -\frac{\psi_T}{P_1}
\end{aligned}$$

Where:

$$\mathrm{N} = F_1P_4P_5 + F_2\tau P_5 + F_3P_4\gamma_T + F_3\tau\gamma_C$$

and

$$Q_1 = \sigma_T + \mu_H, \quad P_1 = \psi_1 + \mu_H, \quad P_2 = \theta_T + \mu_H, \quad P_3 = \tau + \gamma_T + \delta_T + \mu_H$$
$$P_4 = \gamma_C + \delta_T + \mu_H, \quad P_5 = \alpha_T + \delta_T + \mu_H$$

Substituting the values of the parameters into the expressions of the sensitivity analysis of the tuberculosis model above, we obtain the sensitivity indices of the model as presented below:

$$-\Im_{\beta_T}^{\mathrm{R}_0} = 1, \Im_{\theta_T}^{\mathrm{R}_0} = 0.999911, \Im_{\tau}^{\mathrm{R}_0} \approx 0.000732, \Im_{\gamma_T}^{\mathrm{R}_0} \approx 0.4333, \Im_{\alpha_T}^{\mathrm{R}_0} = -0.8261$$
$$\Im_{\omega}^{\mathrm{R}_0} = -0.6667, \Im_{\eta_1}^{\mathrm{R}_0} \approx 0.0253, \Im_{\eta_2}^{\mathrm{R}_0} \approx 0.000146, \Im_{\eta_3}^{\mathrm{R}_0} \approx 0.0243, \Im_{\sigma_T}^{\mathrm{R}_0} = -0.8571$$
$$\Im_{\gamma_C}^{\mathrm{R}_0} \approx -0.6313, \quad \Im_{\psi_T}^{\mathrm{R}_0} = -0.99988$$

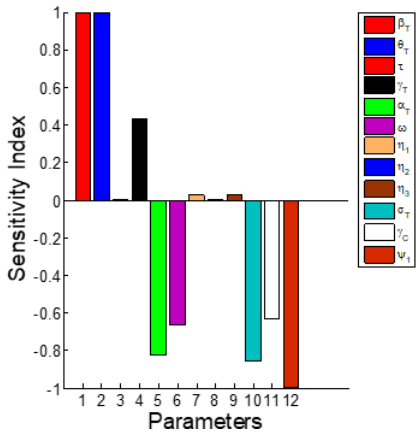

Figure 2: Sensitivity bar chart

Based on the sensitivity bar chart, parameters with positive sensitivity indices such as the contact rate between susceptible and infected humans are identified as drivers that increase the basic reproduction number (R_0). In the context of tuberculosis (TB), a high contact rate implies that infected individuals are more likely to transmit the disease to susceptible individuals through close interactions, shared air in confined spaces, or inadequate infection control practices. Consequently, R_0, which quantifies the average number of secondary infections generated by a single infected individual in a wholly susceptible population, rises when the contact rate increases [23]. Therefore, public health strategies aimed at reducing contact, such as isolation of infectious patients, improved ventilation, wearing masks, and public education on cough hygiene, can significantly lower the value of R_0, ultimately aiding in TB control. Conversely, parameters with negative sensitivity indices, such as the treatment rate and the impact of environmental factors, tend to decrease R_0 when improved. An increased treatment rate means more infected individuals are being diagnosed and receiving timely, effective therapy, which not only reduces their infectious period but also prevents complications and transmission. As treatment accelerates recovery and reduces the bacterial load in the environment, R_0 declines. Therefore, strengthening access to diagnostics, ensuring adherence to Directly Observed Therapy (DOT), and improving drug availability are critical in controlling the spread of TB [21]. These environmental factors, when improved (e.g., through better housing, ventilation systems, and cleaner air), can lower TB transmission rates and thus reduce R_0. For instance, improving natural ventilation in homes and health facilities can greatly reduce the concentration of TB bacilli in the air. Consequently, the sensitivity analysis suggests that interventions targeting both contact reduction and environmental improvements are as crucial as

medical treatment for effective TB control. parameters with positive sensitivity indices amplify R_0 and thus exacerbate TB spread; these should be minimized [22].

Meanwhile, parameters with negative sensitivity indices suppress R_0 and should be optimized through targeted interventions. Reducing the contact rate and enhancing treatment coverage and environmental conditions together create a multifaceted approach that effectively reduces TB transmission potential.

10 Data Fitting for model

To align the collected data with the mathematical sub-models for malaria and tuberculosis, the study employed the fmincon optimization function from MATLAB's Optimization Toolbox. This approach is specifically designed for solving constrained nonlinear optimization problems, making it well-suited for calibrating complex disease models. The primary goal of using fmincon was to determine the optimal set of parameters that minimize the difference between the model's output and actual epidemiological data [19]. By reducing this discrepancy, the fitting process significantly improves the model's accuracy in replicating real-world disease dynamics. Through this optimization technique, the model's parameters were fine-tuned to ensure that simulated outputs closely matched the observed data trends [20]. This not only strengthens the model's reliability but also enhances its predictive power for evaluating intervention strategies. The effectiveness of this parameter-fitting process is illustrated in the figures below, where a clear visual comparison is made between the simulated and observed data [28, 29]. These visualizations validate the model's ability to capture the underlying transmission patterns of both diseases and highlight the robustness of the optimization procedure used.Tuberculosis (TB) data fitting refers to the process of aligning mathematical models with actual disease data in order to uncover key insights about TB transmission and evaluate the effectiveness of control measures. This involves adjusting model parameters so they closely match observed data, enabling researchers to estimate important epidemiological metrics such as the effective reproduction number and treatment success rates [27]. Through this process, the validity of the model's assumptions can be tested, and reliable predictions about future trends can be made. Additionally, it aids in designing and implementing more efficient TB control and elimination strategies. The annual number of confirmed TB cases from 2014 to 2021 is presented below, based on records from the Global Tuberculosis Program [18].

Table 3: Tuberculosis data

Year	Cases
2014	550,000
2015	650,000
2016	750,000
2017	800,000
2018	900,000
2019	$1,000,000$
2020	$1,250,000$
2021	$1,100,000$

Source:[32] WHO 2023 https://www.who.int/publications/i/item/9789240067754

The tuberculosis (TB) data presented in Table 3, collected from the World Health Organization (WHO), provides a crucial foundation for statistical modeling and data fitting [32]. This data-set likely includes yearly or regional TB case counts, incidence and mortality rates, and possibly subcategories such as drug-resistant TB and TB/HIV co-infections. Using this data for fitting involves applying mathematical or statistical models such as linear regression, time series analysis, or logistic model to understand trends, make predictions, or evaluate the effectiveness of interventions.

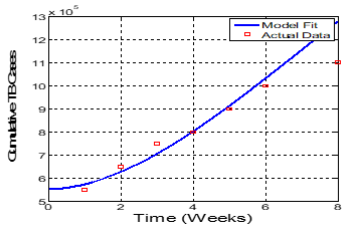

Figure 3: Data fitting for the TB model

The figure 3 presents the data fitting results for tuberculosis (TB), comparing the model's simulated predictions (represented by the solid blue line) with the actual observed case data (shown as red square markers) over a series of weeks. The fitting was achieved using the fmincon function in MATLAB to optimize the model parameters, ensuring that the model closely reflects real-world observations. As shown in the graph, there is a strong agreement between the model output and the actual data, particularly from the middle to later weeks, indicating that the model effectively captures the underlying transmission dynamics of TB. The curve follows a nonlinear, exponential-like growth pattern, which is characteristic of TB spread in populations without sufficient control measures. While minor deviations are observed in the early weeks, they remain within acceptable limits, reflecting the inherent variability in reported epidemiological data. Overall, the close alignment between the model and the observed data highlights the reliability of the parameter estimation process and confirms the model's suitability for predicting TB trends and evaluating the potential impact of intervention strategies.

11 Graphs of Numerical Simulations Of The Tuberculosis Model

Numerical simulations play a crucial role in mathematical modeling, especially for complex systems like infectious disease transmission, where analytical solutions may be difficult or impossible to obtain. They allow researchers to visualize the dynamic behavior of a model over time, assess the impact of varying parameters, and predict possible outcomes under different intervention scenarios. Through simulations, one can evaluate how factors such as vaccination, treatment, contact rates, or environmental changes influence disease progression and control. This provides valuable insights into threshold conditions like the basic reproduction number (R_0) and helps identify critical points where policy or behavioral interventions can be most effective. Ultimately, numerical simulations serve as a powerful tool for translating theoretical models into practical, data-driven strategies for public health planning and decision-making.

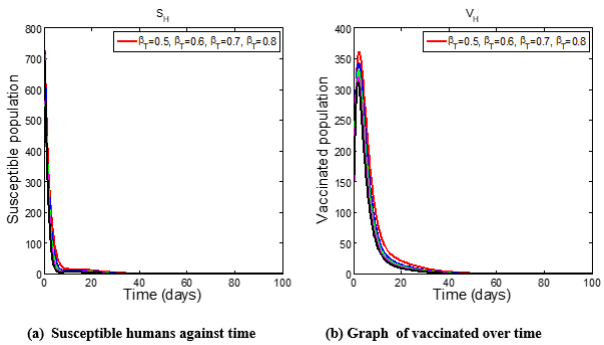

(a) Susceptible humans against time (b) Graph of vaccinated over time

Figure 4: Graph of Susceptible and Vaccinated classes

Figure 4a displays the dynamics of the susceptible human population (SH) over time under different transmission rates ($\beta_T = 0.5, 0.6, 0.7,$ and 0.8). The graph shows a rapid decline in the susceptible

Table 4: Parameters Table of Values Used for the Study

Parameter	Values	Sources
Λ_H	0.00011	[32]
β_T	0.334	Fitted
K_T	0.8333	[32]
θ_T	0.45	Fitted
μ_H	0.00004	[32]
γ_T	0.62	Fitted
τ	0.001000	Fitted
δ_T	0.10000	Fitted,
α_T	0.76000	Fitted
α_T	0.800	Fitted
ω	0.50	Fitted
ζ_T	0.20	Fitted

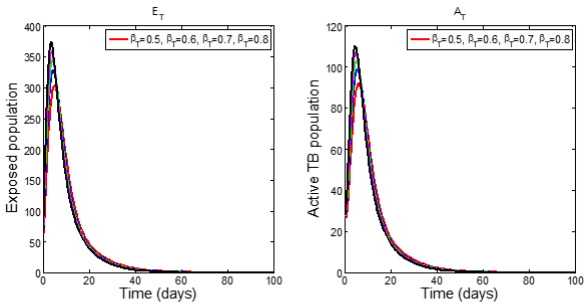

(a) Graph of exposed population (b) Graph of acute TB population

Figure 5: Graph of Exposed and Acute TB classes

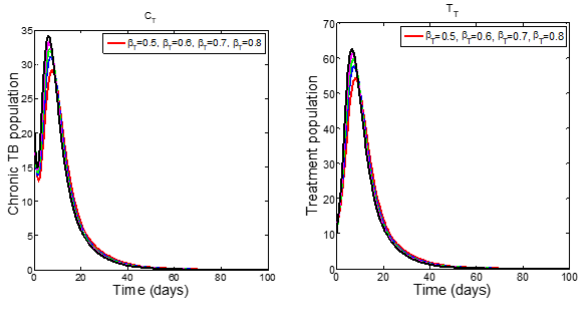

(a) Graph of chronic TB population (b) Graph of treatment class

Figure 6: Graph of Chronic and Treated TB classes

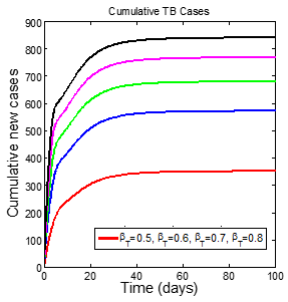

Figure 7: Graph of cumulative cases

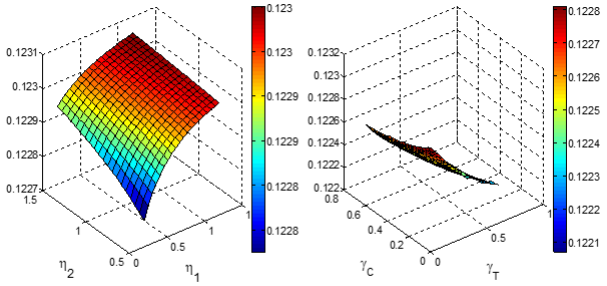

(a) Effect of η_1 and η_2 on R_0 (b) Effect of γ_T and γ_c on R_0

Figure 8: Graph of the effect of η_1, η_2, γ_T and γ_C on R_0

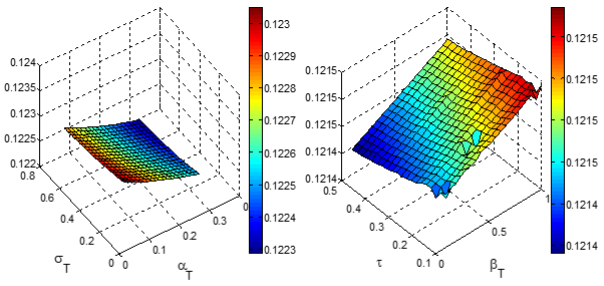

(a) Effect of varying σ_T and α_T on R_0 (b) Effect of varying τ and β_T on R_0

Figure 9: Graph of the effect of varying ρ_T, α_T, τ and β_T on R_0

population during the first 20 days, followed by stabilization at low levels approaching zero as time progresses to 100 days. Higher values of β (transmission rate) result in steeper initial declines, illustrating how increased transmissibility accelerates the depletion of susceptible individuals. This represents the classic pattern of susceptible depletion during disease spread, where susceptible individuals either become infected or vaccinated. The rapid decrease indicates an efficient transmission process of tuberculosis within the population, suggesting that preventive interventions need to be implemented early to maintain a substantial proportion of protected individuals. Figure 4b illustrates the vaccinated human population (VH) dynamics over time. The graph shows an initial increase reaching a peak around days $3-5$, followed by a continuous decline toward zero. The different β values produce similar curve patterns but with notable variations in peak heights and decay rates. Higher transmission rates correspond to slightly lower peaks in the vaccinated population, likely because more individuals transition directly to exposed status before vaccination. From an epidemiological perspective, the declining vaccination curve indicates that vaccinated individuals are either losing their immunity over time or transitioning to other compartments in the model. The relatively quick disappearance of the vaccinated population suggests a need for booster programs or improved vaccine efficacy to maintain protection against tuberculosis.

Figure 5a represents the exposed human population (ET) over time. The curves show a characteristic epidemic wave with rapid growth to peaks between days 5-10, followed by a progressive decline. The peak is highest for $\beta = 0.8$ (black line) and progressively lower for decreasing β values. This pattern demonstrates how transmission intensity directly affects the number of individuals exposed to but not yet infectious with tuberculosis. Epidemiologically, the exposed population represents a critical hidden reservoir of potential future cases. The time lag between exposure peak and subsequent infectious peaks illustrates the latency period of tuberculosis infection, highlighting the challenge of early detection and the importance of prophylactic treatment for exposed individuals before they become infectious. Figure 5b shows the active tuberculosis cases (AT) over time. Similar to the exposed population, it displays epidemic waves with peaks occurring slightly later than those of the exposed population, around days $8-12$. The highest peak corresponds to $\beta = 0.8$, with progressively lower peaks for lower transmission rates. The curves demonstrate how active TB cases emerge from the exposed population following the latency period. From an epidemiological standpoint, these curves represent the clinically detectable burden of disease. The lag between exposure and active disease highlights the challenge of tuberculosis control by the time cases are detected, substantial transmission may have already occurred. The eventual decline suggests that, without reintroduction, tuberculosis outbreaks will eventually burn out once susceptible individuals are depleted.

Figure 6a depicts chronic tuberculosis cases (CT) over time. The pattern mirrors that of active cases but with lower magnitudes, peaking around days 8-12 before gradually declining. Higher transmission rates correspond to higher peaks of chronic cases. This graph illustrates how a proportion of active cases transition to a chronic state, representing individuals with persistent infection. Epidemiologically, chronic cases are significant as they represent a long-term reservoir of infection that can be difficult to eliminate. These individuals may experience recurring symptoms and require extended treatment regimens. The parallel shapes between active and chronic cases suggest a consistent progression rate from active to chronic tuberculosis regardless of transmission intensity. Figure 6b presents the treatment population (TT) over time. The curves show initial growth to peaks around days 8-12, closely following the patterns of active and chronic cases, before declining toward zero. Higher transmission rates result in higher treatment numbers. This pattern represents the healthcare system's response to identified cases. Epidemiologically, the treatment curves illustrate the burden on healthcare systems and resource requirements during an outbreak. The eventual decline suggests successful treatment outcomes, but the delay between disease peaks and treatment peaks highlights the challenge of rapidly identifying and treating all cases. The shape similarity across different transmission rates indicates that treatment capacity scales with case numbers in this model. Figure 7 displays cumulative tuberculosis cases over time for different transmission rates. Unlike previous graphs showing instantaneous populations, this graph shows a monotonically increasing function that eventually plateaus. Higher transmission rates

correspond to higher final cumulative case counts, with $\beta = 0.8$ resulting in approximately 850 cases and $\beta = 0.5$ resulting in only about 350 cases. This dramatic difference underscores how small changes in transmission rates can substantially impact the total disease burden. Epidemiologically, this represents the overall impact of the outbreak in terms of total affected individuals. The plateauing indicates the eventual containment of the outbreak, while the final values provide a measure of the total epidemic size. The substantial differences based on transmission rates demonstrate the potential impact of even modest reductions in transmission through public health interventions.

Figure 8a presents a 3D surface plot examining the relationship between parameters η_1 and η_2 and the basic reproductive number for TB transmission. The surface demonstrates how they jointly influence TB transmission dynamics. The gradient from blue to red indicates increasing values of the epidemiological metric as both parameters increase. From an epidemiological perspective, this suggests that these parameters have a positive correlation with disease spread potential. The relatively narrow range of values ($0.1227 - 0.1231$) indicates that variations in these parameters produce subtle yet consistent effects on tuberculosis transmission dynamics. This relationship could be useful for fine-tuning intervention strategies if these parameters represent controllable factors in tuberculosis management. Figure 8b illustrates the relationship between γ_T (treatment rate of humans infected with acute TB) and γ_{o} (treatment rate of humans infected with chronic TB) and the epidemic threshold metric. The diagonal gradient shows that higher values of γ_T combined with lower values of γ_{o} produce higher values of the response variable. Epidemiologically, this reveals important insights about treatment prioritization. The pattern suggests that increasing treatment rates for acute TB cases has a more substantial positive impact on epidemic control than increasing treatment rates for chronic cases. This finding has significant implications for public health resource allocation, indicating that targeting and treating acute TB cases promptly could potentially yield better epidemiological outcomes than focusing equivalent resources on chronic cases. The relationship likely stems from interrupting transmission chains earlier when acute cases are treated promptly. Figure 9a displays how σ_T and α_T influence the epidemic metric, where α_{t} represents the recovery rate of humans from TB treatment. While σ_T wasn't explicitly defined in your parameter list, the surface shows a clear gradient from lower values (blue) when both parameters are low to higher values (red) when both parameters are high. This indicates that improvements in both treatment recovery rates and the parameter σ_T work synergistically to affect TB dynamics. From a public health perspective, this highlights the importance of not only initiating treatment but ensuring successful completion and recovery. The consistent gradient without plateaus suggests that improvements in recovery rates continue to yield benefits across the examined parameter range, supporting investment in comprehensive treatment follow-up programs and patient support to maximize recovery outcomes. Figure 9b shows the relationship between τ (rate at which acutely infected humans progress to chronic TB) and β_T (effective contact rate with probability of infection per contact). The surface indicates that higher transmission rates (β_T) combined with lower progression rates to chronic infection (τ) correspond to slightly higher values of the epidemic metric. This relationship reveals an important dynamic in TB epidemiology: the disease's spread is more sensitive to its transmission rate than to the rate at which acute cases become chronic. The small irregularities in the surface might represent threshold effects where particular combinations of transmission and progression create distinct epidemiological scenarios. From a control perspective, this suggests that interventions reducing the overall transmission rate (such as improved ventilation, masks, or reduced crowding) may be more effective than interventions aimed solely at preventing progression from acute to chronic disease states

12 Conclusion

This study offers a comprehensive mathematical framework for understanding and controlling tuberculosis (TB) by integrating both biomedical and environmental intervention strategies. The model incorporates essential components such as vaccination, treatment, isolation, reinfection, improved ventilation, environmental disinfection, and public health education elements that are often underrepresented

in traditional TB models. By deriving the basic reproduction number (R_0) using the next-generation matrix approach, the study establishes clear threshold conditions for disease elimination. Stability analyses of the disease-free and endemic equilibria, alongside robust numerical simulations, confirm the model's predictive accuracy and validate its applicability to real-world scenarios. Sensitivity analysis revealed that certain parameters particularly the contact rate between susceptible and infected individuals strongly influence the spread of TB by increasing R_0. This highlights the urgent need for public health measures aimed at reducing interpersonal contact in high-risk settings, such as through isolation, improved ventilation, mask usage, and hygiene education. Conversely, parameters with negative sensitivity indices, such as treatment rates and environmental quality, were found to significantly reduce R_0 when improved. Timely diagnosis, access to quality treatment, adherence to DOT programs, and environmental interventions (like improved housing and air circulation) emerged as key drivers in reducing transmission. The findings underscore that TB control cannot rely solely on medical interventions; rather, it requires an integrated approach combining effective treatment with behavioral, structural, and environmental strategies. Importantly, the model also emphasizes the value of data fitting using localized and real-time surveillance data to enhance model relevance and guide context-specific policy decisions. In conclusion, this work demonstrates that integrating biomedical and environmental strategies within a mathematically grounded framework significantly enhances our ability to predict, manage, and ultimately reduce the burden of TB. Future research should focus on improving the TB model by using region-specific data to increase accuracy and relevance. Studies should also consider the influence of socio-economic factors like healthcare access and urban crowding. Incorporating stochastic methods and machine learning can enhance real-time forecasting and outbreak detection. Evaluating the cost-effectiveness of intervention strategies is important for better resource allocation. Additionally, future models should address co-infections (such as TB-HIV) and drug-resistant TB to provide a more complete understanding of TB dynamics and control.

References

[1] Zumla, A., George, A., Sharma, V., Herbert, N., & Baroness Masham of Ilton. (2013). WHO's 2013 global report on tuberculosis: successes, threats, and opportunities. The Lancet, 382(9907), 1765-1767. https://doi.org/10.1016/S0140-6736(13)62072-4

[2] World Health Organization. (2023). Global tuberculosis report 2023. https://www.who.int/publications/i/item/9789240076729

[3] Pai, M., Kasaeva, T., & Swaminathan, S. (2022). Covid-19's devastating effect on tuberculosis care-a path to recovery. New England Journal of Medicine, 386(16), 14901493. https://doi.org/10.1056/NEJMp2118145

[4] Escombe, A. R., Oeser, C. C., Gilman, R. H., Navincopa, M., Ticona, E., Pan, W., ... & Evans, C. A. (2007). Natural ventilation for the prevention of airborne contagion. PLoS Medicine, 4(2), e68. https://doi.org/10.1371/journal.pmed. 0040068

[5] Knight, G. M., McQuaid, C. F., Dodd, P. J., & Houben, R. M. G. J. (2019). Global burden of latent multidrug-resistant tuberculosis: trends and estimates based on mathematical modelling. The Lancet Infectious Diseases, 19(8), 903-912. https://doi.org/10.1016/S1473-3099(19)30307-X

[6] Yuen, C. M., Amanullah, F., Dharmadhikari, A., Nardell, E. A., Seddon, J. A., Vasilyeva, I., & Becerra, M. C. (2015). Turning off the tap: stopping tuberculosis transmission through active case-finding and prompt effective treatment. The Lancet, 386(10010), 2334-2343. https://doi.org/10.1016/S0140-6736(15)00322-0

[7] Arinaminpathy, N., Dowdy, D., & Dye, C. (2016). How do delays in diagnosis affect TB transmission? Trends in Microbiology, 24(7), 538-540. https://doi.org/10.1016/j.tim.2016.03.006

[8] Kimbrough, W., Saliba, V., Dahab, M., Haskew, C., & Checchi, F. (2012). The burden of tuberculosis in crisis-affected populations: a systematic review. The Lancet Infectious Diseases, 12(12), 950-965. https://doi.org/10.1016/S1473-3099(12)70225-6

[9] Mangtani, P., Abubakar, I., Ariti, C., Beynon, R., Pimpin, L., Fine, P. E., ... & Rodrigues, L. C. (2014). Protection by BCG vaccine against tuberculosis: a systematic review of randomized controlled trials. Clinical Infectious Diseases, 58(4), 470-480. https://doi.org/10.1093/cid/cit790

[10] Tait, D. R., Hatherill, M., Van Der Meeren, O., Ginsberg, A. M., Van Brakel, E., Salaun, B., ... & McShane, H. (2019). Final analysis of a trial of M72/AS01E vaccine to prevent tuberculosis. New England Journal of Medicine, 381(25), 2429-2439. https://doi.org/10.1056/NEJMoa1909953

[11] Menzies, D., Joshi, R., & Pai, M. (2007). Risk of tuberculosis infection and disease associated with work in health care settings. The International Journal of Tuberculosis and Lung Disease, 11(6), 593-605. https://pubmed.ncbi.nlm.nih.gov/17519089/

[12] Dye, C., Garnett, G. P., Sleeman, K., & Williams, B. G. (1998). Prospects for worldwide tuberculosis control under the WHO DOTS strategy. The Lancet, 352(9144), 1886-1891. https://doi.org/10.1016/S0140-6736(98)03199-7

[13] Mukandavire, Z., Gumel, A. B., Garira, W., & Tchuenche, J. M. (2009). Mathematical analysis of a model for TB with environmental contamination. Mathematical Biosciences & Engineering, 6(3), 661-687. https://doi.org/10.3934/mbe.2009.6.661

[14] Barman, M., Panja, M., Mishra, N., & Chakraborty, T. (2025). Epidemic-guided deep learning for spatiotemporal forecasting of tuberculosis outbreak. Machine Learning, 114, Article 213. https://doi.org/10.1007/s10994-025-06848-4

[15] Kasereka, M. (2024). Multi-level modeling of tuberculosis dynamics using coupled agent-based and equation-based models. Infectious Disease Modelling, 9, 15-27. https://doi.org/10.1016/j.idm.2024.01.004

[16] Xu, Z., Yang, Y., & Li, J. (2024). Modeling tuberculosis dynamics in China under vaccination strategies: Analysis and control. Mathematics and Computers in Simulation, 216, 24-39. https://doi.org/10.1016/j.matcom.2023.11.016

[17] Abonyo, D. O., & Okeyo, J. K. (2025). Optimal control and cost-effectiveness analysis of tuberculosis with environmental transmission: A case study of Kenya. BMC Infectious Diseases, 25(1), 114. https://doi.org/10.1186/s12879-025-08249-z

[18] Akinyemi, L., Yusuf, M., & Olanrewaju, S. (2024). Mathematical modeling of tuberculosis dynamics and control strategies in Nigeria. Journal of Applied Mathematics and Computation, 430, 127312. https://doi.org/10.1016/j.amc.2024.127312

[19] Collins, O. C., & Duffy, K. J. (2022). A mathematical model for the dynamics and control of malaria in Nigeria. Infectious Disease Modelling, 7(4), 728-741. https://doi.org/10.1016/j.idm.2022.10.005

[20] Anyanwu, M. C., & Mbah, G. C. E. (2021). Stability analysis of a mathematical model for the use of Wolbachia to stop the spread of Zika virus disease. Biometrical Letters, 58(1), 41-58. https://doi.org/10.2478/bile-2021-0003

[21] Atokolo, W, & Mbah, G. C. E. (2020). Modeling the control of Zika virus vector population using the sterile insect technology. Journal of Applied Mathematics, 2020, Article ID 6350134, 12 pages. https://doi.org/10.1155/2020/6350134

[22] Odeh, J. O, Agbata, B. C, Ezeafulukwe, A. U, Madubueze, C. E, Acheneje, G. O., & Topman, N. N. (2024). A mathematical model for the control of chlamydia disease with treatment strategy. Journal of Mathematical Acumen and Research, 7(1), 45-60. https://www.researchgate.net/publication/381278254

[23] Agbata, B. C., Obeng-Denteh, W., Amoah-Mensah, J., Kwabi, P. A., Shior, M. M., Asante-Mensa, F., & Abraham, S. (2024). Numerical solution of fractional order model of measles disease with double dose vaccination. Dutse Journal of Pure and Applied Sciences (DUJOPAS), 10(3b), 202-217. https://www.ajol.info/index.php/dujopas/article/view/281624

[24] Bolaji, B., Onoja, T., Agbata, B C., Omede, B. I., & Odionyenma, U. B. (2024). Dynamical analysis of HIV-TB co-infection transmission model in the presence of treatment for TB. Bulletin of Biomathematics, 2(1), 21-56. https://doi.org/10.59292/bulletinbiomath.2024002

[25] Acheneje, G. O., Omale, D., Agbata, B. C., Atokolo, W., Shior, M. M., & Bolawarinwa, B. (2024). Approximate solution of the fractional order mathematical model on the transmission dynamics of the co-infection of COVID-19 and Monkeypox using the Laplace-Adomian decomposition method. International Journal of Mathematics and Statistics Studies, 12(3), 17-51. https://eajournals.org/ijmss/vol12-issue-3-

[26] Agbata, B. C., Agbebaku, D. F., Odo, C. E., Ojih, J. T., Shior, M. M., & Ezugorie, I. G. (2024). A mathematical model for the transmission dynamics of COVID-19 in Nigeria and its post-effects. International Journal of Mathematical Analysis and Modelling, 7(2), 523-547. https://tnsmb.org/journal/index.php/ijmam/article/view/191

[27] Ugwu, K. O., Onah, I. S., Mbah, G. C., & Ezeonu, I. M. (2020). Rifampicin resistance patterns and dynamics of tuberculosis and drug-resistant tuberculosis in Enugu, South Eastern Nigeria. Journal of Infection in Developing Countries, 14(9), 1011-1018. https://doi.org/10.3855/jidc.12736

[28] Duru, E. C., Mbah, G. C. E., Anyanwu, M. C., & Topman, N. N. (2024). Modelling the co-infection of malaria and Zika virus disease. Journal of the Nigerian Society of Physical Sciences. Advance online publication. https://doi.org/10.46481/jnsps.2024.1938

[29] Agbata, C. B., Meco, Z. M., Agbebaku, D. F., Dervishi, R., & Ezike, M. G. C. Fractionalorder analysis of malaria and tuberculosis co-dynamics: A Laplace Adomian decomposition approach. Edelweiss Applied Science and Technology, 9(4), 1675-1714 (2025). https://doi.org/10.55214/25768484.v9i4.6353

[30] Agbata, B. C., Cenaj, E., Agbebaku, D. F., Collins, O. C., Dervishi, R., Emadifar, H., Ezeafulukwe, A. U., & Mbah, G. C. E. Mathematical analysis of the transmission dynamics of malaria and tuberculosis co-infection with control strategies. Engineering Reports, 7(6), e70210. (2025). https://doi.org/10.1002/eng2.70210

[31] Akowe, E., Ahman, Q. O., Agbata, B. C., Joseph, S. O., Senewo, E. O., Danjuma, A. Y., & Yahaya, D. J. A novel malaria mathematical model: Integrating vector and non-vector transmission pathways. BMC Infectious Diseases, 25, Article 322. (2025). https://doi.org/10.1186/s12879-025-10653-8

[32] World Health Organization. (2023). Global tuberculosis report 2023. World Health Organization. https://www.who.int/publications/i/item/9789240067754

13 APPENDIX

13.1 Local Asymptotic Stability of the Disease Free Equilibrium Point of TB Model

The Jacobian matrix of the tuberculosis model is given as

$$J = \begin{bmatrix} -Q_1 & 0 & 0 & -F_1 & -F_2 & -F_3 & \varsigma_T \\ \sigma_T & -P_1 & 0 & 0 & 0 & 0 & 0 \\ 0 & \psi_T & -P_2 & F_1 & F_2 & F_3 & 0 \\ 0 & 0 & \theta_T & -P_3 & 0 & 0 & 0 \\ 0 & 0 & 0 & \tau & -P_4 & 0 & 0 \\ 0 & 0 & 0 & \gamma_T & \gamma_C & -P_5 & 0 \\ 0 & 0 & 9 & 0 & \alpha_T & 0 & -P_6 \end{bmatrix}$$

The characteristic polynomial of the jacobian matrix of the system is given as

$$\begin{aligned}
&\lambda^7 - (-P_6 - P_5 - P_4 - P_3 - P_2 - P_1 - Q_1)\,\lambda^6 \\
&- (-P_6 - P_5 - P_4 - P_3 - P_2 - P_1 - Q_1)\,\lambda^6 - 9P_3P_4\psi_T\sigma_T\varsigma_T - 9P_3P_5\psi_T\sigma_T\varsigma_T - 9P_4P_5\psi_T\sigma_T\varsigma_T \\
&- \begin{pmatrix} F_1\theta_T - P_1P_2 - P_1P_3 - P_1P_4 - P_1P_5 - P_1P_6 - P_1Q_1 - P_2P_3 \\ -P_2P_4 - P_2P_5 - P_2P_6 - P_2Q_1 - P_3P_4 - P_3P_5 - P_3P_6 - P_3Q_1 \\ -P_4P_5 - P_4P_6 - P_4Q_1 - P_5P_6 - P_5Q_1 - P_6Q_1 \end{pmatrix}\lambda^5 \\
&+ (F_1P_1P_4P_5P_6\theta_T - F_1P_1P_4P_5Q_1\theta_T - F_1P_1P_4P_6Q_1\theta_T - F_1P_1P_5P_6Q_1\theta_T \\
&- F_1P_4P_5P_6Q_1\theta_T + F_1P_4P_5\psi_T\sigma_T\theta_T + F_1P_4P_6\psi_T\sigma_T\theta_T + F_1P_5P_6\psi_T\sigma_T\theta_T \\
&- F_2P_1P_5P_6\tau\theta_T - F_2P_1P_5Q_1\tau\theta_T - F_2P_1P_6Q_1\tau\theta_T - F_2P_5P_6Q_1\tau\theta_T \\
&+ F_2P_5\tau\psi_T\sigma_T\theta_T + F_2P_6\tau\psi_T\sigma_T\theta_T - F_3P_1P_4P_6\gamma_T\theta_T - F_3P_1P_4Q_1\gamma_T\theta_T \\
&- F_3P_1P_6Q_1\gamma_T\theta_T - F_3P_1P_6\tau\gamma_C\theta_T - F_3P_1Q_1\tau\gamma_C\theta_T - F_3P_4P_6Q_1\gamma_T\theta_T \\
&+ F_3P_4\gamma_T\psi_T\sigma_T\theta_T - F_3P_6Q_1\tau\gamma_C\theta_T + F_3P_6\gamma_T\psi_T\sigma_T\theta_T + F_3\tau\gamma_C\psi_T\sigma_T\theta_T \\
&+ P_1P_2P_3P_4P_5P_6 + P_1P_2P_3P_4P_5Q_1 + P_1P_2P_3P_4P_6Q_1 + P_1P_2P_3P_5P_6Q_1 \\
&+ P_1P_2P_4P_5P_6Q_1 + P_1P_3P_4P_5P_6Q_1 + P_2P_3P_4P_5P_6Q_1 - \tau\alpha_T\psi_T\sigma_T\theta_T\varsigma_T \\
&- (F_1P_1\theta_T + F_1P_4\theta_T + F_1P_5\theta_T + F_1P_6\theta_T + F_1Q_1\theta_T + F_2\tau\theta_T + F_3\gamma_T\theta_T \\
&-P_1P_2P_3 - P_1P_2P_4 - P_1P_2P_5 - P_1P_2P_6 - P_1P_2Q_1 - P_1P_3P_4 - P_1P_3P_5)\,\lambda^4 \\
&+ \begin{pmatrix} F_1P_1P_4\theta_T + F_1P_1P_5\theta_T + F_1P_1P_6\theta_T + F_1P_1Q_1\theta_T \\ +F_1P_4P_5\theta_T + F_1P_4P_6\theta_T + F_1P_4Q_1\theta_T + F_1P_5P_6\theta_T + F_1P_5Q_1\theta_T + F_1P_6Q_1\theta_T - F_1\psi_T\sigma_T\theta_T \\ +F_2P_1\tau\theta_T + F_2P_5\tau\theta_T + F_2P_6\tau\theta_T + F_2Q_1\tau\theta_T n \\ +F_3P_1\gamma_T\theta_T + F_3P_4\gamma_T\theta_T + F_3P_6\gamma_T\theta_T + F_3Q_1\gamma_T\theta_T + F_3\tau\gamma_C\theta_T n \\ -P_1P_2P_3P_4 - P_1P_2P_3P_5 - P_1P_2P_3P_6 - P_1P_2P_3Q_1 \end{pmatrix}\lambda^3 \\
&+ \begin{pmatrix} ((F_1P_4 + F_1P_5 + F_1Q_1 + F_2\tau + F_3\gamma_T)\,P_1 + (F_1P_4 + F_1P_5 + F_2\tau + F_3\gamma_T)\,Q_1 + (F_1P_5 + F_3\gamma_T)\,P_4 \\ +\tau\gamma_C F_3 + \tau F_2P_5 - \psi_T\sigma_T F_1 \\ +((F_1P_4 + F_1P_5 + F_2\tau + F_3\gamma_T)\,Q_1 + (F_1P_5 + F_3\gamma_T)\,P_4 + \tau\,(F_2P_5 + F_3\gamma_C))\,P_1 \end{pmatrix}\lambda^2 \\
&+ F_1P_4P_5P_6\psi_T\sigma_T\theta_T + F_2P_5P_6\tau\psi_T\sigma_T\theta_T \\
&+ F_3P_4P_6\gamma_T\psi_T\sigma_T\theta_T + F_3P_6\tau\gamma_C\psi_T\sigma_T\theta_T - P_5\tau\alpha_T\psi_T\sigma_T\theta_T\varsigma_T \\
&- 9P_3P_4P_5\psi_T\sigma_T\varsigma_T + P_1P_2P_3P_4P_5P_6Q_1\,(1 - R_{0T})
\end{aligned}$$

Applying the Routh Hurwitz criterion,

$\implies (1 - R_{0T}) > 0$ and hence $R_{0T} > 1$